PCCP

KINETIC ENERGY RELEASE DISTRIBUTIONS FROM DISSOCIATIVE PHOTOIONIZATION OF WEAKLY BOUND TRIMERS AT 14-27 eV

Journal:	*Physical Chemistry Chemical Physics*
Manuscript ID	CP-ART-05-2018-003013.R1
Article Type:	Paper
Date Submitted by the Author:	25-Jul-2018

Complete List of Authors:	Cheng, Bing-Ming; National Syncrotron Radiation Research Center (NSRRC), Scientific Research Division Grover, J.; Brookhaven National Laboratory, Upton, NY 11973 Walters, E.; University of New Mexico, Chemistry Clay, J.; University of New Mexico

KINETIC ENERGY RELEASE DISTRIBUTIONS FROM DISSOCIATIVE PHOTOIONIZATION OF WEAKLY BOUND TRIMERS AT 14-27 eV

B.-M. Cheng[1]*, J.R. Grover[2]*, E. A. Walters[3]* and J. T. Clay[3]

[1]*National Synchrotron Radiation Research Center, 101 Hsin-Ann Road, Hsinchu Science Park. Hsinchu 30076, Taiwan; bmcheng@nsrrc.org.tw*

[2]*Department of Chemistry, Brookhaven National Laboratory, Upton, NY 11973; jrobbgrover@cs.com*

[3]*Department of Chemistry, University of New Mexico, Albuquerque, NM 87131; edandsuewalt@earthlink.net*

(Received May xx, 2018; accepted xxxx xx, 201X)

ABSTRACT

The formation of the intriguing ions $C_4H_6O^+$, $C_6H_6Cl^+$, and $C_6H_6O^+$, by dissociative ionization of heterotrimers of butadiene/sulfur dioxide, benzene/hydrogen chloride and benzene/oxygen by 14 – 27 eV photons, illustrates the possibility that VUV irradiation of clusters comprised of three or more molecules could provide a route to make ions containing bonds not previously accessible. Kinetic energy release distributions were measured in an attempt to understand the formation of these ions and why clusters larger than dimers are needed. Standard theory was applied to find whether more complicated theoretical treatments are needed to understand the data. It was found that all of the above ions were most likely produced by essentially the same mechanism: excitation of one moiety, transfer of its excitation energy to the moiety that dissociates, followed by slow decay of the remaining excited ion into the unexcited moiety as the "solvent" plus the ion with the new bond.

The very low reaction probabilities to produce these ions, combined with very low target densities in the presence of many orders of magnitude higher densities of other molecules, precluded the usual imaging techniques. However, we found that the retarding-potential method can give useful data. Also, at present laser photon energies higher than 15 eV provide significantly smaller average intensities than are needed.

INTRODUCTION

Dissociation of even simple molecules by vacuum ultraviolet (VUV) light can open decomposition pathways inaccessible at lower energies. For example, it has recently been shown that molecular oxygen can be produced directly from CO_2 with VUV photons. This is a complex process that requires intramolecular cleavage of two C-O bonds and formation of an O_2 triple bond following absorption of a single photon.[1]

Similarly, formation of the unexpected cations $C_6H_6Cl^+$, $C_6H_6O^+$, and $C_4H_6SO^+$ from the heterotrimers $(C_6H_6)_2{\cdot}HCl$, $(C_6H_6)_2{\cdot}O_2$, and $(C_4H_6)_2{\cdot}SO_2$, respectively, by dissociative photoionization in the single-photon energy range of 14-27 eV has been observed.[2-5] Each of these photocations contains at least one bond not found in the target cluster. Photon energies at the onsets for these ions lie well above the ionization threshold of any of the cluster constituents, so involvement of high-energy levels, such as Rydberg states,[6-9] and energy surface roaming[1,10] is feasible. Nevertheless, mechanisms for product ion formation consistent with the experimental results were proposed that consisted of direct ionization of one of the organic moieties in each cluster to an excited state followed by a rapid set of energy transfer and rearrangement steps to give a "hot" solvated ionic complex which decomposed to the product ion in a slow unimolecular event of boiling off the solvent molecule. A reasonably sensitive test of this mechanism is the measurement of the photocation kinetic energy release distributions (KERDs) as demonstrated, for example, by Baer et al. ,[6] who used the TPEPICO technique to measure KERDs for understanding dissociative ionization of molecular clusters. We report here the measurement of KERDs for the three ionic products, $C_6H_6Cl^+$, $C_6H_6O^+$, and $C_4H_6SO^+$, and an analysis of the KERDs based on a phase-space theory approach to the slow step.[11-15]

KERDs can be measured by ion imaging techniques whenever they can be applied.[7,8] Challenges presented by these three cations are: high photon energies required, low target cluster densities and low ion product cross sections. The very energetic onsets for the ions means that photon energies in excess of 15 eV must be used. A molecular beam rich in trimer target species can only be made at low cluster densities and even then the beam consists of a mixture of related clusters. The low cross sections resulted in product ion counting rates of 0.01 to 0.1 sec^{-1}, whereas total counting rates of all ions frequently reached 10^6 sec^{-1}. These constraints preclude ion imaging.

On the other hand, synchrotron radiation has high photon fluxes above 15 eV. By sacrificing energy resolution to optimize ion counting rates, a retarding potential method allowed determination of KERDs for the target ions with energy resolutions of about 10% up to 200 meV. The observed KERDs were compared with those calculated on the basis of the mechanism described above and assumptions for product ion structure. Matches sufficiently close between the observed and calculated distributions support the proposed mechanism.

Our apparatus was calibrated by measuring the KERD of the predissociation of the $\tilde{C}\ \sum_g^+$ state of CO_2^+ to produce CO. Yields of 22±3% and 78±3% to form the v=0 and v=1 states, respectively, were obtained, in reasonable agreement with Eland's result.[16]

EXPERIMENT

The facility used for this work was the normal incidence monochromator of the U-11 beam line at the 750 MeV electron storage ring of the National Synchrotron Light Source at Brookhaven National Laboratory.[2-4]

Retarding potential device. A retarding potential device was built incorporating a lens system to focus the energy-discriminated ions onto the entrance slit of a quadrupole mass spectrometer. Detailed design, a compromise between ion transmission efficiency and energy resolution, was carried out using the ion-trajectory program SIMION.[17] The resulting electrode arrangement is diagrammed in Fig. 1. The analyzer is cylindrical, 30.0 mm in diameter, 59 mm in length. The molecular beam enters and exits electrode V_1 through circular apertures 0.64 mm and 2.0 mm in diameter, respectively. Synchrotron radiation crosses the molecular beam at 90 degrees, entering through a slot 0.92 x 6.5 mm and leaving via a slot 2.0 x 9.5 mm. These slots accommodate the 66-milliradian horizontal and 9-milliradian vertical divergence of the radiation. With a monochromator slit width of 0.8 mm the resulting crossing zone of radiation and molecular beam is roughly spherical, 0.2 mm^3 in volume.

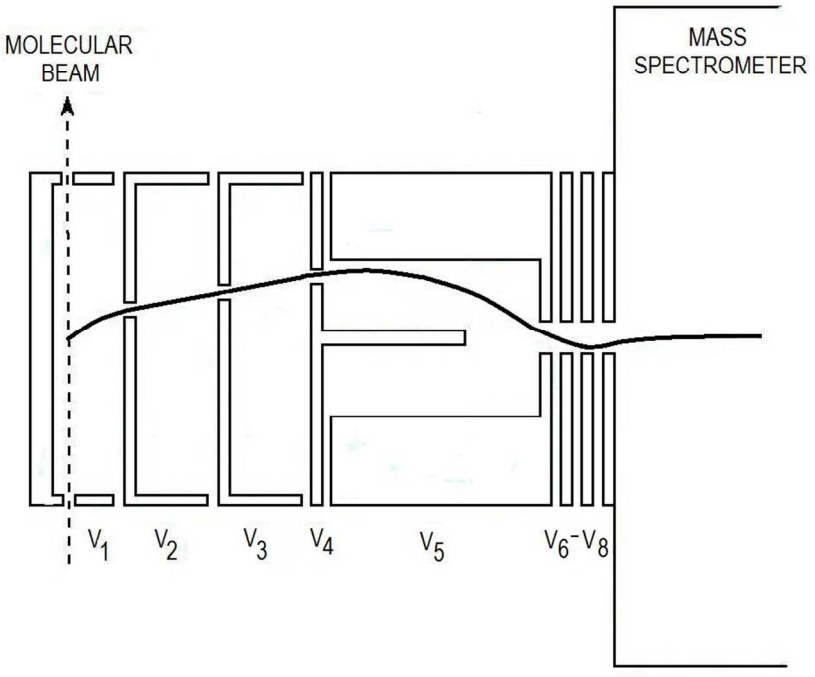

Fig. 1. Basic structure of the kinetic energy analyzer. The heavy black line is a representative ion trajectory. The beam of ionizing radiation intersecting the molecular beam is perpendicular to the plane of the diagram.

The analyzing slit is a centered annular slot in electrode V_4, 1.2 mm wide and subtending an angle of 90°. This slot's inner edge is 5.1 mm from the centerline. Electrodes V_2 and V_3, also with 90°-wide annular slots, maintain field uniformity and allow small steering corrections. The combination of electrode V_5 and the centerline rod of electrode V_4 is a cylindrical lens which brings the ions to the entrance slit of the mass spectrometer. This rod is 1.6 mm in diameter and 13.0 mm long. The distance from the V_4 annulus to the V_5 slit is 20.3 mm. Electrodes V_6 and V_7 then optimize the angles of ion injection into the mass spectrometer. V_8 is the mounting plate, screwed to the mass spectrometer housing, and at ground potential.

Details not shown in Fig. 1: pump-out apertures for electrodes V_2 to V_5, insulators of Delrin® that separate and align the electrodes, the flanges, standoffs and bolts that clamp the assembly together, electrical attachments to the power supply for electrodes V_2 to V_7, and leads for a thermocouple. All electrodes were fabricated of SS 304 and plated with gold.

The apparatus must operate well above room temperature, 60° C or higher. Severe distortions of signal occur at room temperature, evidently the result of surface-charging effects.

Scanning product ion energies required sweeping the seven different electrode voltages simultaneously, in such a way as to optimize ion transmission.

The detected ions must be generated within 10^{-7} seconds after the photoelectron is ejected. SIMION calculations show delayed ions are transmitted with substantially reduced efficiency. Also, their contributions to the distribution are broader, and at apparent laboratory energies considerably lower than if they had been prompt. RRKM calculations (see appendix of Ref. (**17**)) for the reactions being studied here give lifetime upper limits much shorter than 10^{-7}

seconds, even for cluster dissociation energies of 60 kJ mol^{-1}. Metastable precursors are highly unlikely. The device of Fig. 1 was installed in the apparatus described previously.[18,19]

Calibration. Calibration of the analyzer was accomplished by preparation of atomic beams containing argon atoms of known kinetic energies through jet expansion of a series of helium-argon mixtures at 500 Torr followed by photoionization at 700 Å (17.7 eV) to produce argon ions. Velocity focusing of the expansion and the lack of a component from dissociation yielded a sharply peaked velocity distribution at kinetic energies calculated via the expression

$$E_x(<W>) = (5/2)R(T_n-T_b)[40.0/<W>] \quad (1)$$

where R is the gas constant, $<W>$ is the average molecular weight of the He/Ar mixture, T_n is the nozzle temperature (297 K), and T_b is the beam temperature (2.6 K).[19] The proportions of the mixtures used ranged from Ar:He = 1:0 to 1:39, giving argon ion kinetic energies from 63.4 to 518 meV.

A plot of the nominal energy $E_n(<W_i>)$, the "instrument reading", for mixtures $<W_i>$ versus the experimental calibration energy $E_x(<W_i>)$ evaluated from Eq. (1) is given in Fig. 2(a). Here, $E_n(<W_i>)$ is the minimum in the first differential of the signal intensity I_s with respect to the instrument reading, i.e., the point of steepest descent.

$$E_n = E \text{ at } [dI_s/dE]_{min} \quad (2)$$

Although the relationship is linear the line does not pass through the origin, so a small offset correction is necessary:

$$E_x = aE_n + b = E_l \quad (3)$$

In order to avoid frequent recalibration with Ar/He mixtures internal calibration was carried out for each run using as wide a range of ion masses as possible in that experiment. For example, for

the C_6H_6/O_2 experiments, masses from 16, for O^+, to 156, for $(C_6H_6)_2^+$, were used. Here, Eq. (1) was modified to include rotational and vibrational energy.

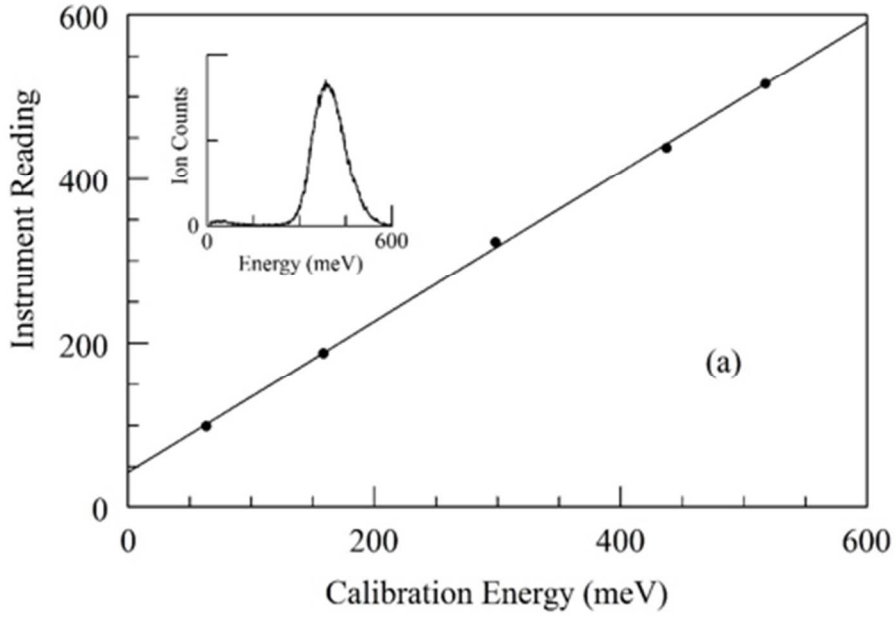

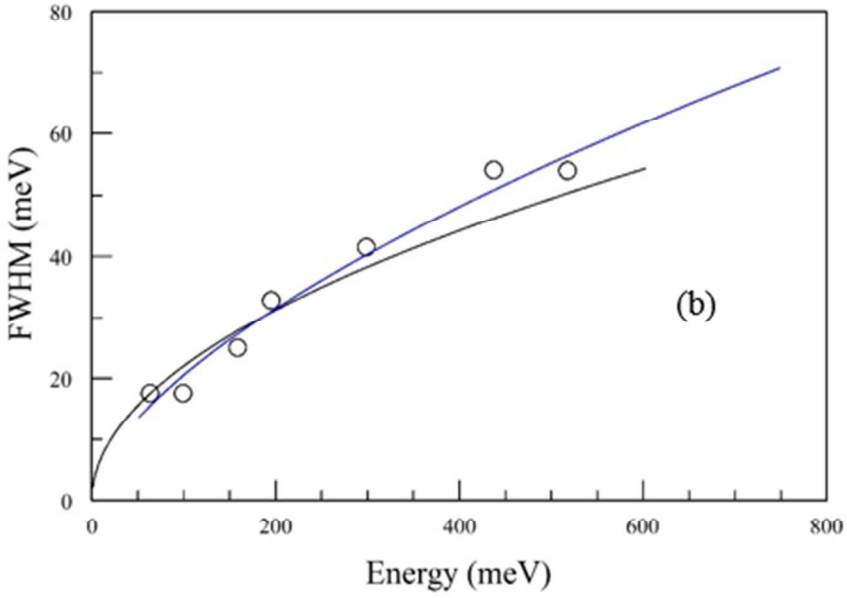

Fig. 2. (a) Relationship between energies calculated from the applied voltages (ordinate), and the translational energies of the ionized argon atoms (abscissa). Inset: raw energy spectrum of Ar^+ for He:Ar=19:1. (b) Energy resolution: experimental (points and blue line) versus theoretical (black line).

For each run the laboratory energies, E_l, are calculated from the nominal energies, E_n, by Eq. (3). This spectrum is then corrected for the decay of the ring current (i.e., of the radiation intensity), and for the separately measured background.

The contribution of thermal species to the background must be addressed. Consider the inset in Fig. 2(a). Here the main peak is the raw signal obtained for He:Ar = 19:1, where the photoion has virtually no kinetic energy from dissociation. The signal in the thermal region, below 30 meV translational energy, is less than 1% of that in the main peak. It includes several contributions, such as tailing from the main peak, stray argon in the instrumental chamber, cosmic rays, stray ions of other masses that leak through the mass filter, and any thermal (unaccelerated) argon in the molecular beam. The most important contribution is expected to be the stray argon, because, as described above, the device samples a 1.0 mm-diameter beam entering the experimental chamber. Geometry dictates that 7% of the beam atoms enter the analyzer and the balance of the argon atoms are scattered into the experimental chamber. Since these stray argon atoms have a mean energy of about 80º C (30 meV) inside the heated analyzer, slower than the beam argon atoms by a factor of about 0.26, they are $0.26^{-1} \cong 4$ times more likely to be ionized than the beam atoms. Offsetting this, three quarters of the strays move backwards or sidewise in the instrument, making them undetectable, thereby reducing their effective ionization rate by a factor four. Thus, it is likely that the stray Ar atoms are responsible for most of the signal below 50 meV. In turn this means that a thermal (23º C) contribution to the composition of the core of the nozzle beam itself is very much smaller than 1%.

The nominal ion-energy resolution, determined as the full width at half maximum of the negative wing of the first differential, is shown in Fig. 2(b), where the blue line is the least-squares log-log straight-line fit. The actual resolution is better than this, especially at the higher energy end, because our measurements include the intrinsic width of the argon-ion calibration beams, which were velocity focused by the jet expansion to a FWHM of about 10%.[20] The black line is the theoretical resolution for isotropic breakup of excited ions. This was calculated via SIMION for assumed dissociation energies. Experiment and theory agree well.

Test. Dissociative photoionization of CO_2 proceeds as follows:

$$CO_2 + h\nu \rightarrow CO + O^+ + e. \qquad (4)$$

Photoionization at 19.372 eV (640.0 Å) populates the $\tilde{C}\,\Sigma_g^+$ state of CO_2^+ just at the top of the step in the yield function for the production of O^+. Eland found,[16] using 584 Å radiation, that this state predissociates entirely, within 10^{-6} seconds, into $O^+(^4S_u)$ and $CO(^1\Sigma_g^+)$, 80-95% of which populates the v =1 state, the remaining 5 to 20% populating v = 0. The energetic relationships are summarized in Fig. 3. Resolution of these two bands is a useful test of the apparatus.

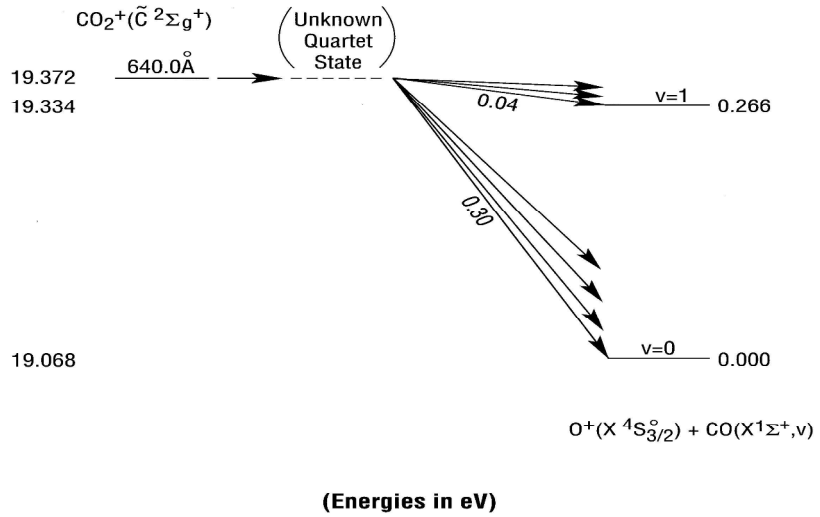

Fig. 3. Energetic relationships in the dissociative ionization of carbon dioxide at 640.0 Å (19.372 eV). The labels 0.04 and 0.30 give the expected maximum translational energies, in eV, to the v = 1 and v = 0 levels, respectively.

Figure 4(a) shows the result (points) of an experiment using a jet expansion of CO_2:He = 1:19 at 500 Torr and observing O^+. A second experiment, 33 months later, gave essentially identical results. The solid curve is the energy spectrum of CO_2^+, taken under the same conditions, shifted and scaled to the peak of the O^+ to indicate the spectrum expected for a kinetic energy release of zero. The steepness of descent of its high-energy side indicates the resolution. The substantially increased width of the O^+ spectrum and changes in slope near 500-600 meV reveal the kinetic energy release.

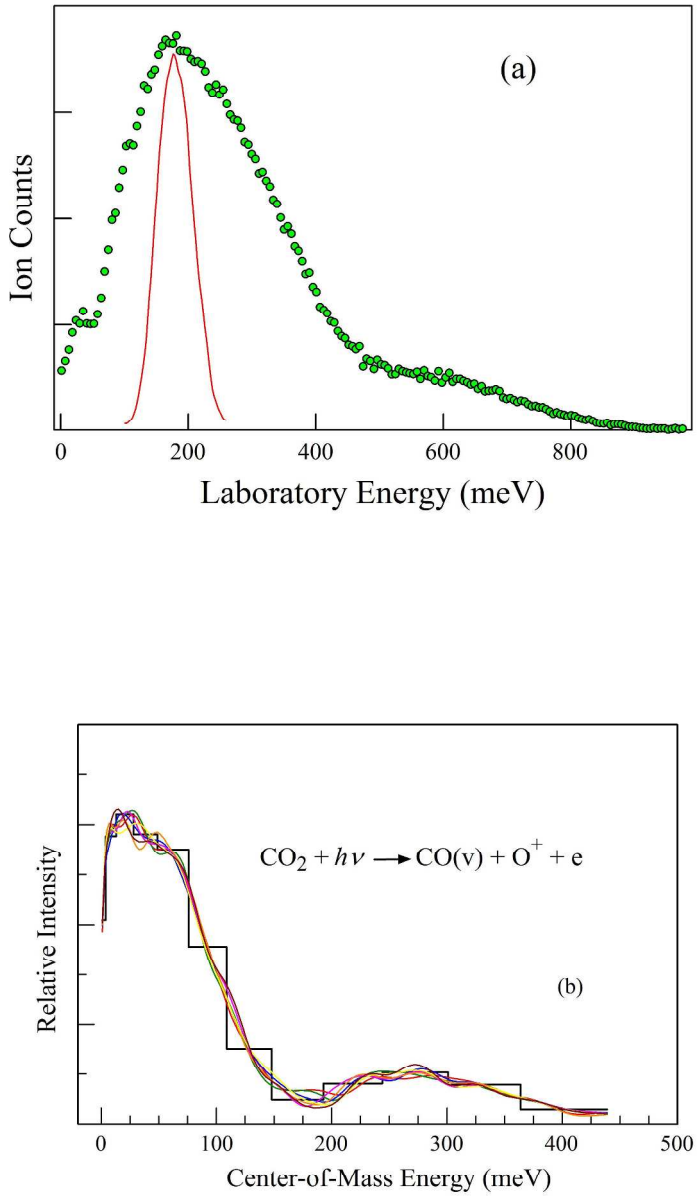

Fig. 4. (a) Points: measured raw energy distribution of O^+ from the photoionization of CO_2 at 640.0 Å (19.372 eV) in the jet-expanded mixture CO_2:He = 1:19, at 500 Torr. Line: raw energy distribution of CO_2^+, scaled down in energy and adjusted in intensity to allow comparison of its shape with the O^+ data. (b) Black steps: kinetic energy release distribution of CO_2 + hν (640.0 Å) → CO + O^+ + e, calculated from the raw energy distribution shown in (a) combined with a second measurement of the same distribution. Colored curves: see text.

Determination of the KERD involves differentiating the data in Fig. 4(a). The scatter due to counting statistics required some smoothing of the data, however only as much smoothing was used as necessary to bring out the major features of the function. The result is the spectrum in Fig. 4(b). The required value of V_B was calculated from the laboratory energy maximum of the O^+ spectrum. The experimental result is represented by the black step function. Although the calculated experimental result is in the form of a continuous function, it was rendered into steps to indicate the experimental resolution according to the measured FWHM of the energy resolution, given in Fig. 2(b). The solution retains uncertainties due to the statistical scatter of the points. An estimate of the uncertainty in the relative intensities was obtained as follows. The uncertainty of the count at each experimental point was taken to be the square root of its value multiplied by 1.1. This was then multiplied by randomly chosen -1 or +1 and the result was added to the count. This synthetic data set was then fit as before. The process was repeated to give a total of seven different synthetic "data" sets, each shown as a curve with a different color in Fig.4(b).

We indeed see two peaks, at ~50 and ~280 meV, near the energies expected for the rovibrational bands of neutral carbon monoxide at v = 0 and v = 1, which have upper limits at 39 and 305 meV (Fig. 4(b)). The apparent resolution is less good than that measured for Ar/He (Fig. 2(b)). However, some of the observed width probably comes from unresolved rotational distributions. Roaming may also be involved.[1,10] Integration of the peaks in our two experiments gives the population of the v = 0 state as 20 and 25%, i.e., an average of 22±3%, in agreement with Eland's result. That the observed spectrum is reasonable allows an additional conclusion: the dissociation occurs within 10^{-7} seconds, decreasing Eland's limit of 10^{-6} seconds.

Reagents. The reagents used for the experiments, argon, hydrogen chloride, oxygen, sulfur dioxide, 1,3-butadiene, and benzene, were all commercial materials of standard research grade. The techniques and conditions for making the cluster beams of benzene/oxygen,[3] benzene/hydrogen chloride,[2,21] and butadiene/sulfur dioxide [4,21] have been described.

RESULTS AND DISCUSSION

$C_4H_6SO^+$: The KERD of $C_4H_6SO^+$ was measured in the nozzle expansion of a 1:4 C_4H_6:SO_2 mixture at a pressure of 750 Torr and a wavelength of 600 Å (20.66 eV). The KERD is the black steps in Fig. 5. Prior experiments showed that at 750 Torr $C_4H_6SO^+$ is produced almost entirely from trimers (≥ 96%).[4] Here $<\varepsilon>$ is 44 meV and ε_{max} is 7 meV, both larger than for all the other ions of the butadiene/sulfur dioxide system (Table 1). A substantial amount of product excitation, including possible isomerization accompanies the formation of $C_4H_6SO^+$ by the 20.7-eV photon, since $<\varepsilon>$ released to both or all products, about 0.2 eV, is far less than the 1.4 eV minimum excess energy implied by the onset at 15.36 eV.[4] There is no clear structure above the maximum at 7 meV, i.e., no evidence of a high barrier or strong repulsion. The KERD is consistent with a statistically guided process.

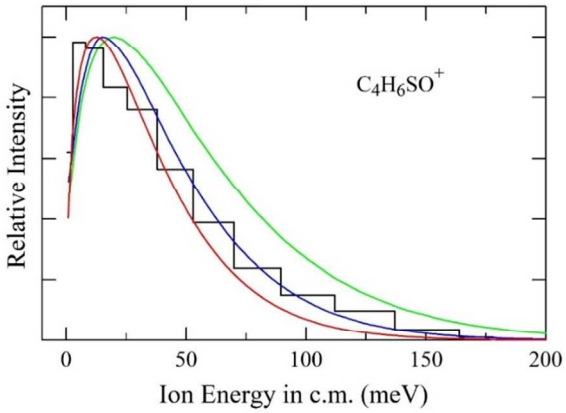

Fig. 5. Comparison of experimental results for $C_4H_6SO^+$ (black steps) with calculations.

Discussion. C_4H_6 in the trimer $(C_4H_6)_2SO_2$ is likely to be the chromophore because the observed onset of 15.36 eV is below the $SO_2 \rightarrow SO^+ + O$ threshold of 15.98 eV,[22] but is well above the energy of ionizing the heterotrimer, ~ 9.0 eV. This suggests that C_4H_6 is ionized to an excited state, $C_4H_6^{+*}$, with sufficient energy above the ground level of the ion to dissociate an S-O bond of the SO_2 cluster constituent via intracluster energy transfer. In neutral SO_2, this would be 5.66 eV for a total of about 14.7 eV of the 15.36 eV available from the ionizing photon at threshold.[23]

A mechanism for producing $C_4H_6SO^+$, consistent with these energetics, is:

$$(C_4H_6)_2SO_2 + h\nu \rightarrow (C_4H_6)(C_4H_6^{+*})SO_2 + e \quad (6a)$$

$$(C_4H_6)(C_4H_6^{+*})SO_2 \rightarrow (C_4H_6)(C_4H_6^{+})(SO_2^*) \quad (6b)$$

$$(C_4H_6)(C_4H_6^{+})(SO_2^*) \rightarrow (C_4H_6{\bullet}C_4H_6)^{+}{\bullet}SO + O \quad (6c)$$

$$(C_4H_6{\bullet}C_4H_6)^{+}{\bullet}SO \rightarrow (C_4H_6{\bullet}C_4H_6{\bullet}SO)^{+*} \quad (6d)$$

$$(C_4H_6{\bullet}C_4H_6{\bullet}SO)^{+*} \rightarrow C_4H_6 + C_4H_6SO^{+} \quad (6e)$$

Photoionization of a C_4H_6 moiety to a high-lying state of the ion, $C_4H_6^{+*}$, is followed quickly by a series of steps to give the excited ionic complex $(C_4H_6 \bullet C_4H_6 \bullet SO)^{+*}$, which yields the product ion $C_4H_6SO^+$ through a slow unimolecular decomposition, Eq. (6e). As a test we attempt to reproduce the KERD, black steps, depicted in Fig. 5, by applying Lorquet's phase-space formulation[11-14] to this final step. We compare the calculation for two product isomers: *cyclic*-$C_4H_6SO^+$ (2,5-dihydrothiophene 1-oxide ion), and *n*-$C_4H_6SO^+$ ($CH_2CHC(SO)CH_3$ ion). The threshold for the former is 13.1 eV, and is 14.1 eV for the latter (see Table 2). The vibrational frequencies for butadiene and sulfur dioxide are those from Shimanouchi.[24] Frequencies for *cyclic*-$C_4H_6SO^+$ were adapted from those for thiophene.[25] Frequencies for linear structures assumed for $C_4H_6SO^+$ and C_4H_6O, (i.e., $CH_2CHCOCH_3$), were taken from compounds having similar groups.[24]

The result for *n*-$C_4H_6SO^+$ is consistent with the experimental KERD above about 30 meV if the recoil of the eliminated oxygen atom is small. See Fig. 5. Here, the red line is for zero recoil from oxygen elimination, and the blue line is for a recoil of 10 meV, half the 20 meV reported in the 193-nm photodissociation of SO_2.[26]

The calculated distribution for *cyclic*-$C_4H_6SO^+$ deposits too much translational energy in the product ion (with 10-meV first-step recoil), as shown by the green line.

An analogous calculation was carried out in which SO_2 is the chromophore in an initial photoionization step $SO_2 + h\nu \rightarrow SO^+ + O + e$, and where *n*-$C_4H_6SO^+$ is the product with 10-meV recoil from O-atom elimination. The result, not plotted, is nearly indistinguishable from the green line in Fig. 5.

These calculations fail to give a good account of the intensity below 25 meV. Perhaps thermodynamically less stable structures than 1,3-butadiene might be considered for the C_4H_6 radical in Eq. (6e), but at the expense of a less good fit at the higher energies.

We conclude that the measured KERD for $C_4H_6SO^+$ is roughly consistent with the mechanism presented above in which the slow step is loss of a "solvent" C_4H_6 molecule from the solvated product ion, *n*-$C_4H_6SO^+$.

TABLE 1. Peak (ε_{max}) and average ($<\varepsilon>$) values for the product ion KERDs observed in this study.

Species					
Product	Putative Parent	P_{noz}/Torr	λ/Å	$<\varepsilon>$/meV[b]	ε_{max}/meV[c]
O^+	CO_2	500	640	---	50 280
$C_4H_6^+$	C_4H_6	200 300 400 500 800	600	9.2 9.7 17 20 25	3.0[a] 2.8[a] 3.1[a] 3.0[a] 3.6[a]
$C_4H_6^+$	C_4H_6	500	1300	7.1	2.1[a]
$C_4H_5^+$	C_4H_6	200	600	15	3.9
$(C_4H_6•SO_2)^+$	$C_4H_6•SO_2$	500 800	1300 600	15 30	2.3[a] 4.7
$C_4H_6SO^+$	$C_4H_6•SO_2$	700	600	44	7
$(C_6H_6)_2^+$	$(C_6H_6)_2$	800 2000	700 700	40 58	5 23
$C_6H_6O^+$	$(C_6H_6)_n•O_2$ n=1,2,…	2000 2000	750 600	64 77	13 16
$(C_6H_6•O_2)^+$	$C_6H_6•O_2$	1300 2000	700 700	16 18	4.8 4.4
$(C_6H_6•HCl)^+$	$(C_6H_6)_n•HCl$ n=1,2,…	325	735	31	11
$C_6H_6Cl^+$	$(C_6H_6)_2•HCl$	325	735	63	21

[a] Regarded as lower limit, because less than the resolution of 3.5 meV
[b] Experimental uncertainty of $<\varepsilon>$ is ± 10%, mostly systematic error
[c] Experimental uncertainty of ε_{max} is ± 25%, dominated by the limited number of counts

TABLE 2. Heats of formation [a] used in the calculations.

species	$\Delta_f H^o$ / kJ mol^{-1}		Reference
	neutral	ion	
H	216.0		c
O(^{3}P)	246.8	1560.7	c
O(^{1}S)	651.0		o
CO($^1\Pi$)	664.7		c,p
Cl	119.6	1371	c
SO	5.0	1000.7	c
SO_2	-294.3	894	c
SO_3	-390.0	845	c
HCl	-92.1	1137.7	c
s-trans 1,3-C_4H_6	124	999	g
C_4H_6O (CH_2=$CHCOCH_3$)	-121		h
chain-C_4H_6SO	38	912	i
C_5H_6 (cyclopentadiene)	149	975	c,m,t
C_6H_6 (benzene)	100.4	992.6	c
C_6H_6 (1,5-hexadien-3-yne)	369	1189	c
C_6H_6 (1,5-hexadiyne)	432	1387	c
C_6H_7 (cyclohexadienyl radical)	225		d
C_6H_7 (CH≡CCH_2CH_2C≡CH)H	390	1124	b, est

C_6H_5OH (phenol)	-85.2	732	c
C_6H_6O (benzene oxide)	114	928	m,s
C_6H_6O (oxepin)	113	927	m,r
C_6H_6O (butadienyl ketene)	126	888	m,q
C_6H_6O (2,4-cyclohexadienone)	9	899	m,n
$C_6H_6•O_2$	93.7	979	j
ipso-C_6H_6Cl		950	b
para-HC_6H_5Cl		840	h
C_6H_6Cl $(CH≡CCH_2CH_2C≡CH)Cl$			
$(C_4H_6)_2$	238		i
$C_4H_6 \cdot SO_2$	-184	690	i
$C_4H_6(SO_2)_2$	-494	377	i
$(C_4H_6)_2SO$		1025	i
$(C_4H_6)_2SO_2$	-73	795	i
2,5-dihydrothiophene-1-oxide	-8	820	i
2,5-dihydrothiophene-1,1-dioxide	-230	740	h,i
$(C_6H_6)_2$	191	1029	e
$C_6H_5OH•C_6H_6$ (phenol benzene)	-4	812	k
$C_6H_6•C_6H_6Cl^+$		987	b
$C_6H_6•C_6H_6^+•Cl$		1117	b
$(C_6H_6)_2O_2$	184	1067	f
$(C_6H_5OH)_2$ (phenol dimer)	-192	582	k
$(C_6H_6)_2HCl$	79	908	b

$C_6H_6 \bullet C_6H_6^+(^2B_{2u}) \bullet HCl$	1502	b

a At 0 K
b Ref. (**2**), adjusted for the correct value[22] of $\Delta_f H^o_0$(benzene)
c Ref. (**22**)
d Ref. (**31**) Converted to 0 K using reasonable frequencies
e Ref. (**32**), adjusted for the correct value[22] of $\Delta_f H^o_0$(benzene)
f Ref. (**3**). Calculated
g Ref. (**33**), value converted to 0 K; IP from Ref. (**22**)
h 298 K value from Ref. (**22**) converted to 0 K using reasonable frequencies
i Ref. (**4**), or estimated for this work as described in the text
j Ref. (**3**)
k estimated for this work, guided by D(1-naphthol·benzene) = 21.2 kJ mol^{-1}, Ref. (**34**), and D(H_2O·benzene) = 10.2 kJ mol^{-1}, Ref. (**35,36**)
m Ref. (**37**). Theoretical at 298 K.
n ionization potential assumed to be near that of 2-cyclohexen-1-one, 9.23 eV, Ref. (**22**). Estimated correction of +14 kJ mol^{-1} for conversion from 298 K to 0 K.
o Ref. (**38**)
p Ref. (**39**)
q Estimate 7.9 eV for IP, and +11 kJ/mole for conversion from 298 K to 0 K.
r Estimate 8.4 eV for IP, and +11 kJ/mole for conversion from 298 K to 0 K.
s Estimate 8.4 eV for IP, and +11 kJ/mole for conversion from 298 K to 0 K.
t Ref. (**40**). Add an estimated 10 kJ/mole for conversion from 298 K to 0 K.

$C_6H_6Cl^+$: Figure 6 shows, in the black steps, the KERD of $C_6H_6Cl^+$ measured at 735 Å (16.9 eV) using a 1:9 benzene:hydrogen chloride mixture at a nozzle pressure of 325 Torr. At this pressure mixed trimers are abundant because the beam density of C_6H_6•HCl is beyond its maximum at about 250 Torr.[2]

$(C_6H_6$•$HCl)^+$ can be produced by direct ionization of C_6H_6•HCl, while $C_6H_6Cl^+$ can only be produced by fragmentation of trimers or larger clusters,[2] so it is expected that $C_6H_6Cl^+$ generally has more kinetic energy than $(C_6H_6$•$HCl)^+$. This is observed, Table 1, where values of mean product ion kinetic energies, $<\varepsilon>$, and maxima, ε_{max}, for all the species observed in this study are given.

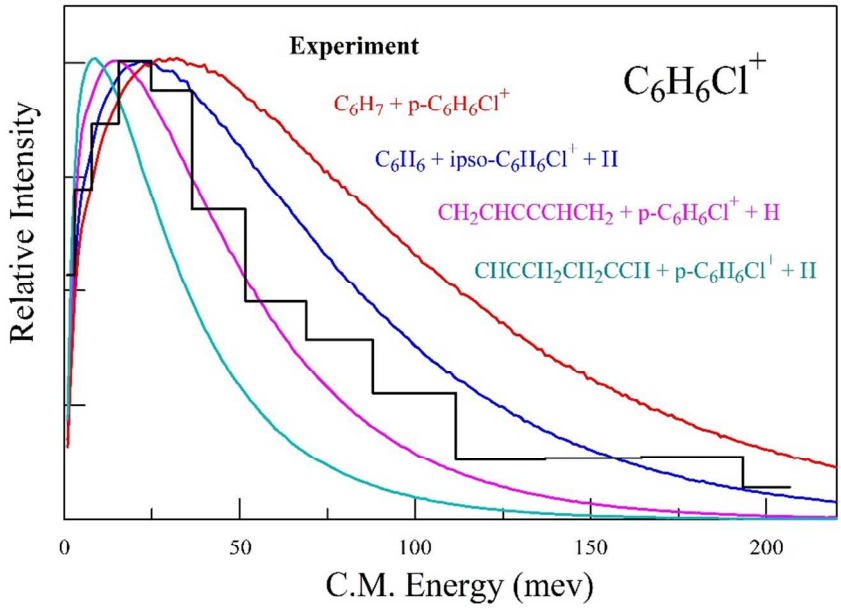

Fig. 6. Comparison of experimental results for $C_6H_6Cl^+$ (black steps) with calculations (colored lines, as labeled).

Discussion. Possible routes to $C_6H_6Cl^+$ must be compatible with the following experimental observations and constraints.

1. The parent cluster is more likely to be $(C_6H_6)_2HCl$ than $C_6H_6(HCl)_2$.[2]

2. The experiment could not distinguish among *ipso*-$C_6H_6Cl^+$ and *ortho-, meta-, para*-$HC_6H_5Cl^+$.

3. The onset is at 14.8 eV, 4.5 eV higher than the lowest possible threshold of 10.26 eV, which is for producing *ipso*-C_6H_7 + *p*-$C_6H_6Cl^+$.[2]

4. Production from $C_6H_6 \cdot HCl$ could not be detected.[2]

5. The H atom of HCl does not appear in the $C_6H_6Cl^+$.[2]

6. Photoionization at 735 Å (16.87 eV) creates ions $(C_6H_6)_2HCl^+$ in a wide range of excitations, from 0 to 8.28 eV, where the ionization potential is 8.59 eV.[2]

7. In this experiment $C_6H_6Cl^+$ is a minor product, ~ 0.01% of the total ion-detection rate, which is dominated by $H^{35}Cl^+$,$H^{37}Cl^+$, $C_4H_4^+$ and $C_6H_6^+$.

8. The average C.M. energy is 63 meV, with the peak at 21 meV.

The mechanism proposed in Ref. 2 implies constraints on the kinetic energy deposited in the product ion. The QET formulation of Lorquet was used to calculate the slow step product kinetic energies, which, again, is taken to be the unimolecular cooling of the excited complex by ejection of a "solvent" molecule. The vibrational level densities of benzene were calculated from the frequencies in Shimanouchi.[24] The thirty-three frequencies for *ipso*-$C_6H_6Cl^+$ were estimated from the modes for benzene, chlorobenzene,[27] and other appropriate species.[24] The rotational constants for benzene were calculated from the ground-state bond lengths[28] and from a reasonable structure[29] for *ipso*-$C_6H_6Cl^+$. The effect of including rotation was found to be much smaller than the experimental uncertainty.

The calculated translational energy-release distributions are compared to the experimental results in Fig. 6. Many fragment sets which are formula-consistent with the breakup of $(C_6H_6)_2HCl^+$ can be envisaged and the question is whether a particular set can be found that matches the experimental data. $CH_2CHCCCHCH_2 + C_6H_6Cl^+ + H$ is nearly such a set. It should be noted that other product sets will also match, the important point being that matches can be found. All the matches involve substantial changes in at least one of the partners. Linear products could be involved, but the option of both products being cyclical is not excluded.

The appearance energy of $C_6H_6Cl^+$ at 14.8 eV is some 6.2 eV above the ionization threshold of C_6H_6 at 8.6 eV. This means that the initial ionization event is to a highly excited state of $C_6H_6^{+*}$. In fact, there is sufficient excitation energy available to dissociate HCl, whose isolated-state dissociation energy is 4.433 eV, accounting for the origin of the observed ejected H atom. This atom could have as much as 6.2 eV – 4.4 eV = 1.8 eV kinetic energy, the balance of which remains in the cluster ion to drive rearrangement and to provide the excess energy to be removed by boiling off a "solvent" C_6H_6 molecule.

QET production of the most stable products of the rearrangement step, predicts a KERD much more energetic than experiment (red line in Fig. 6). There seems to be no immediately obvious reason why these products would need an onset of 14.8 eV, resulting in a lower KERD.

At the opposite extreme, production of linear $CHCCH_2CH_2CCH$ plus ejection of a zero-energy H atom predicts a KERD of significantly less energy than experiment (pale blue line). Thus, ascribing the 14.8-eV onset to inclusion of a linear product ion is not supported by the data.

An intermediate product selection, both molecular products cyclical, dark blue line, predicts a KERD somewhat too high in energy for zero-energy H atoms, but too low for 2-eV H atoms [not plotted but close to the pale blue line].

Since reasonable QET predictions bracket the observed KERD, the proposed mechanism is generally supported by the experiment. Indeed, such close agreement between the observed KERD and the multi-step mechanism is substantial support for this overall mechanism.

The following conclusions are drawn.

1. The observed KERD for C_6H_6 Cl^+ generation is consistent with a multi-step mechanism in which the slow step is unimolecular release of a "solvent" molecule to stabilize the product ion.

2. The neutral reaction products are most likely to be atomic H and an aromatic molecule. Certain linear products are thermodynamically possible, but it is not evident there is sufficient energy in the ionizing photon to both dissociate HCl and to open an aromatic ring.

3. Other competing reactions keep $C_6H_6Cl^+$ production small.

4. The small reaction cross section suggests that the process could be restricted to dominance by only one reaction mechanism.

$C_6H_6O^+$: The KERDs for $C_6H_6O^+$ at P_{noz} of 2000 Torr of a 110:1 oxygen:benzene mixture, at two photon energies; 600 Å (20.66 eV), the maximum of the excitation function for producing this ion,[3] and 750 Å (16.53 eV), as far below the maximum as possible while retaining usable signal levels (i.e., 6.6 and 2.4 eV above the effective onset energy of 14.1 eV)[3] are given as steps in Figs. 7(a) and 7(b). The corresponding $<\varepsilon>$ are 64 and 77 meV.

Discussion. The measurement of KERDs for the dissociative photoionization of $(C_6H_6)_2O_2$ clusters at 750 Å and 600 Å adds a new dimension to information on the production of $C_6H_6O^+$. Earlier work established that production of $C_6H_6O^+$ from the heterodimer $C_6H_6{\bullet}O_2$ was too weak

to be detected,[3] and that its most likely precursors are the clusters $(C_6H_6)_n(O_2)_m$, $n \geq 2$, m=1, because clusters $(C_6H_6)_n(O_2)_m$,m>1 could not be detected.[3] In fact, $(C_6H_6)_2O_2$ is likely the most important parent of $C_6H_6O^+$ for the cluster distribution in the molecular beam used in this work. Even though $C_6H_6O^+$ is a minor product, ~ 1%, its onset was determined to be 14.1 eV (880 Å).[3] Ionization at this onset is to an unknown highly excited state in the cluster $[(C_6H_6)_2O_2^+]^*$.[30]

In light of these observations and the similarity to the generation of $C_4H_6SO^+$ and $C_6H_6Cl^+$ions discussed above, the KERDs were analyzed on the basis of the same general mechanism. That is, initial ionization is the $C_6H_6^+(^2B_{2u})$ state of one of the two C_6H_6 cluster constituents. This is followed quickly by a series of steps involving energy transfer, ejection of an O-atom and rearrangement to an excited complex $(C_6H_6 \bullet C_6H_6 \bullet O)^{+*}$. This experiences a slow unimolecular release of a benzene "solvent" molecule to yield the stable product ion $C_6H_6O^+$.

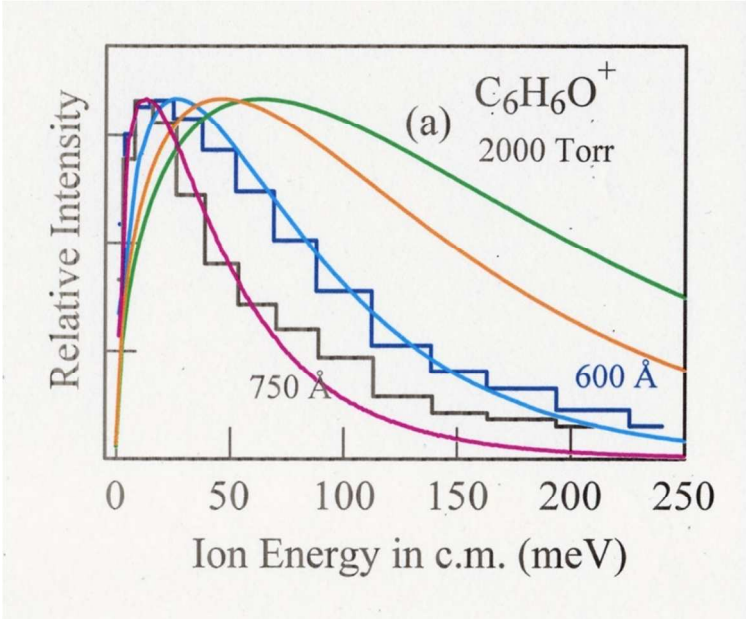

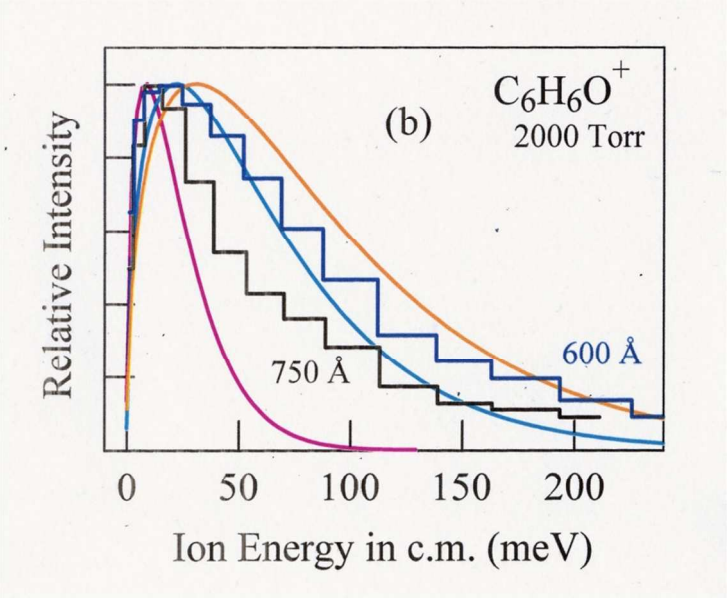

Fig. 7. (a) The blue curve is calculated for 1,5-hexadien-3-yne + phenol ion + O(^{3}P), the violet curve for 2,4-cyclohexadienone + 1,5-hexadien-3-yne ion + O(^{3}P). The green line corresponds to the breakup into phenol and phenol ion, and the yellow line to breakup into oxepin and oxepin ion. (b) Calculated KERDS[11-14,30] for production of benzene + phenol ion + O(^{3}P), yellow curve, + O(^{1}D), blue curve, and O(^{1}S), violet curve. The abscissas in (a) and (b) give the kinetic energy of only the observed ion with respect to the center of mass, not the total kinetic energy of all species in the c.m.

As before, the Lorquet formalism for a unimolecular process was applied to the slow step in the proposed mechanism. The results are found as the colored lines in Figs. 7(a) and 7(b). Dissociation of the ionic complex into neutral and ionic products without loss of an O-atom, phenol and phenol ion (green line) or oxepin and oxepin ion (yellow line), Fig. 7(a), gives KERDs with much more kinetic energy in the product ion than is observed. No known isomers allow agreement with the experiment. If the possibility of O_2 cleavage is included and dissociation is into hydrocarbon fragments, matches with experiment can be made, blue and violet lines, Fig. 7(a). However, these fits require cleavage of aromatic ring bonds in both of the benzene rings, an unreasonable requirement.

For the situation in which the products are benzene and isomers of $C_6H_6O^+$ and a ground-state oxygen atom agreement of the observed and calculated KERDs may be consistent. Also, if the product oxygen atom is formed as $O(^1S)$, too much energy is removed from the system and the observed KERDs have more energetic values than those calculated, Fig 7(b), violet line. KERDs comparable to experiment are calculated when $O(^3P)$ or $O(^1D)$ is produced, together with a benzene "solvent" molecule and phenol cation, i.e., the most stable isomers, Fig 7(b), yellow and blue lines. Once more, agreement between observed and KERDs calculated on the basis of the proposed mechanism is satisfactory and proves to be a rather sensitive test of the mechanism.

CONCLUSION

Kinetic energy release distributions (KERDs) of the three product ions, $C_4H_6SO^+$, $C_6H_6Cl^+$ and $C_6H_6O^+$, made in the dissociative photoionization of their parent trimeric clusters, $(C_4H_6)_2SO_2$, $(C_6H_6)_2HCl$ and $(C_6H_6)_2O_2$, respectively have been measured. The KERDs were analyzed in terms of a common mechanism for formation of the product ions which begins with direct ionization of one of the cluster constituents to an excited state followed rapidly by energy transfer, dissociation of an atom, either H or O, and rearrangement to an excited state. The ionic component of this excited complex is stabilized in a slow unimolecular release of a "solvent" molecule. The mechanism was modelled by applying unimolecular reaction rate theory to the final step. Agreement was found between the experiment and calculated KERDs for all the ionic products. To the extent the same mechanism usually occurs, a general method has been found for forming chemical bonds that are otherwise difficult to make.

ACKNOWLEDGEMENTS

This research was carried out at Brookhaven National Laboratory under contract DE-AC02-76CH00016 with the U.S. Department of Energy and supported in part by its Division of Chemical Sciences, Office of Basic Energy Sciences and in part by the Engineering and Services Laboratory, Air Force Engineering and Services Center, Tyndall AFB, FL 32403. The authors would also like to thank David L. Arneberg and Mary V. Willcox for their support of this work.

REFERENCES AND NOTES

1. Z. Lu, Y.C. Chang, Q-Z. Yin, C.Y. Ng and W.M. Jackson, 2014, *Science* **346**, 61-64.

2. E. A. Walters, J. R. Grover, M. G. White and E. T. Hui, *J. Phys. Chem.*, 1987, **91**, 2758-2762

3. J. R. Grover, G. Hagenow and E. A. Walters, *J. Chem. Phys.*, 1992, **97**, 628-642.

4. J. R. Grover, E. A. Walters, J. K. Newman and M. G. White, *J. Am. Chem. Soc.*, 1990, **112**, 6499-6506.

5. J. R. Grover and E. A. Walters, in *Recent Research Developments in Chemical Physics, V. 3,* ed. S. G. Pandalai, Transworld Research Network, Kerala, 2003, p. 421-455.

6. (a) J. S. Riley and T. Baer, *Mass Spect. & Ion Proc.*, 1994, **131**, 295-305. (b) J. A. Booze and T. Baer, *J. Chem. Phys.*, 1992, **96**, 5541-5543. (c) J. A. Booze, T. N. Feinberg, J. W. Keister and T. Baer, *J. Chem. Phys.*, 1994, **100**, 4294-4299. (d) T. Baer, J. A. Booze and J. R. Riley, *Proc. SPIE*, 1993, **1858**, 158-163.

7. M. N. R. Ashfold, N. H. Nahler, A. J. Orr-Ewing, O. P. J. Vieuxmaire, R. L. Toomes, T. N. Kitsopoulos, I. A. Garcia, D. A. Chestakov, S.-M. Wu and D. H. Parker, 2006, *Phys. Chem. Chem. Phys.* **8**, 26-53.

8. H. Reisler, 2009, *Annu. Rev. Phys. Chem.* **60**, 39-59.

9. P.M. Dehmer and S.T. Pratt, 1982, *J. Chem. Phys.* **76**, 843-853. P.M. Dehmer, 1982, *J. Chem. Phys.* **76**, 1263-1272.

10. A.G. Suits and D.H. Parker, 2014, *Science* **346**, 30-31.

11. P. Urbain, F. Remacle, B. Leyh and J. C. Lorquet, *J. Phys. Chem.*, 1996, **100**, 8003-8007.

12. P. Urbain, B. Leyh, F. Remacle and A. J. Lorquet, *J. Chem. Phys.*, 1999, **110**, 2911-2921.

13. P. Urbain, B. Leyh, F. Remacle and J. C. Lorquet, *Int. J. Mass Spectrom.*, 1999, **185/186/187**, 155-163.

14. J. C. Lorquet, *Int. J. Mass Spectrom.*, 2000, **201**, 59-67.

15. T. Baer and W. L. Hase, *Unimolecular Reaction Dynamics*, Oxford University Press, New York, 1996. See Chs. 7 & 9 (e.g., Eq. (7.45)) and references therein. The authors present a discussion and review of the relationship between patterns of energy disposal and reaction pathways. The appendix contains a computer program for computing densities and sums of ro-vibrational states from molecular frequencies and moments of inertia.

16. J. H. D. Eland, *Int. J. Mass Spectrom. Ion Phys.*, 1972, **9**, 397-406.

17. D. A. Dahl and J. E. Delmore, *EGG-CS-7233, Rev. 2*, Nov. 1987, program SIMION, distributed by Idaho National Engineering Laboratory.

18. M. G. White and J. R. Grover, *J. Chem. Phys.*, 1983, **79**, 4124-4131.

19. J. R. Grover, E. A. Walters, J. K. Newman and M. G. White, *J. Am. Chem. Soc.*, 1985, **107**, 7329-7339.

20. J. R. Grover, Y. Wen, Y. T. Lee and K. Shobatake, *J. Chem. Phys.*, 1988, **89**, 938-946.

21. J. R. Grover, E. A. Walters, D. L. Arneberg and C. Santandrea, *Chem. Phys. Lett.*, 1988, **146**, 305-309.

22. S. G. Lias, J. E. Bartmess, J. F. Liebman, J. L. Holmes, R. D. Levin and W. G. Mallard, *J. Phys. Chem. Ref. Data*, *Suppl. No. 1*, 1988, **17** 1-861. H. M. Rosenstock, K. Draxl, B. W. Steiner and J. T. Herron, *J. Phys. Chem. Ref. Data*, *Suppl. No. 1*, 1977, **6** 1-783.

23. K. Kimura, S. Katsumata, Y. Achiba, T. Yamazaki and S. Iwata, *Handbook of HeI Photoelectron Spectra of Fundamental Organic Molecules*, Halsted Press, New York, 1981.

24. T. Shimanouchi, *Tables of Molecular Vibrational Frequencies*, *Consolidated Vol. 1*, NSRDS-NBS 39, U.S. Govt. Printing Office, Washington, 1972.

25. S. Gronowitz, *V.44: Thiophene and Its Derivatives*, *Part Four*, ed. E.C. Taylor, John Wiley & Sons, New York, 1991, p. 1-294.

26. M. Kawasaki and H. Sato, *Chem. Phys. Lett.*, 1987, **139**, 585-588.

27. D. H. Whiffen, *J. Chem. Soc.*, 1956, 1350-1356.

28. G. Herzberg, *Molecular Spectra and Molecular Structure. III. Electronic Spectra and Electronic Structure of Polyatomic Molecules*, Krieger, Malabar Florida, reprint edition w/corrections, 1991.

29. Five of the carbon and hydrogen atoms are assumed to have the same bond lengths and angles as benzene. The two C-C bond lengths of the sixth ring carbon are assigned to be 1.50 Å. The ring is assumed planar. The hydrogen and ^{35}Cl bonded to the non-benzenoid carbon are assigned bond lengths of 1.07 Å and 1.75 Å, respectively, each bond subtending an angle of 54.5° with respect to the ring plane, the H-C-Cl plane being perpendicular to the ring.

30. The distribution of excitation energy in $[(C_6H_6)_2O_2^+]^*$ is assumed to be constant across the important region from 14.1 to 16.53 eV.

31. Y. Gao, N.J. DeYonker, E.C. Garrett III, A.K. Wilson, T.R. Cundari and P. Marshall, *J. Phys. Chem. A*, 2009, **113**, 6955-6963.

32. J. R. Grover, E. A. Walters and E. T. Hui, *J. Phys. Chem.*, 1987, **91**, 3233-3237.

33. J. D. Cox and G. Pilcher, *Thermochemistry of Organic and Organometallic Compounds*, Academic Press, London and New York, 1970.

34. C. Wickleder, T. Droz, T. Bürgi and S. Leutwyler, *Chem. Phys. Lett.*, 1997, **264**, 257-264.

35. A. Courty, M. Mons, I. Dimicoli, F. Piuzzi, M. P. Gaigeot, V. Brenner, P. de Pujo and P. Millié, *J. Phys. Chem. A*, 1998, **102**, 6590-6600.

36. B.-M. Cheng, J. R. Grover and E. A. Walters, *Chem. Phys. Lett.*, 1995, **232**, 364-369.

37. C. A. Taatjes, D. L. Osborn, T. M. Selby, G. Meloni, A. J. Trevitt, E. Epifanovsky, A. I. Krylov, B. Sirjean, E. Dames and H. Wang, *J. Phys. Chem. A*, 2010, **114**, 3355-3370.

38. J.S. Winn, *Physical Chemistry*, Harper Collins, New York, 1995.

39. G. Herzberg, *Molecular Spectra and Molecular Structure I. Spectra of Diatomic Molecules*, Van Nostrand Reinhold Company, New York, 1950, 534.

40. W.R. Roth, O. Adamczak, R. Breuckmann, H.-W. Lennartz and R. Boese, *Chem. Ber.* 1991, **124**, 2499.

Table of content

Kinetic energy release distributions from dissociative photoionization of weakly bound trimer at 14-27 eV

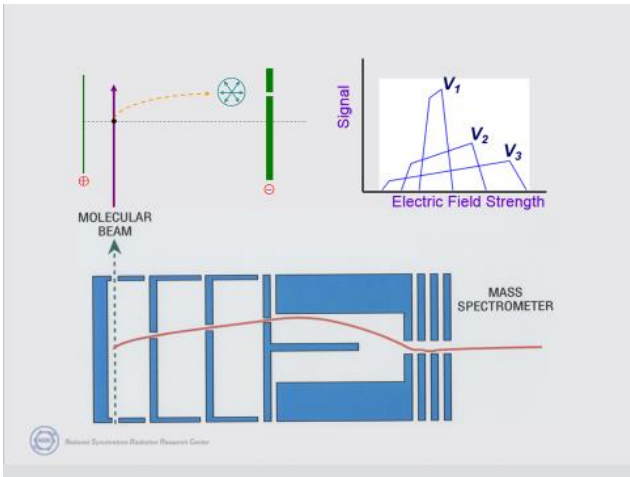

Retarding-potential mass spectrometer coupled to molecular beam measured the kinetic energy release distributions from dissociative photoionization of weakly bound trimer